International Journal of Thermophysics, Vol. 25, No. 3, May 2004 (© 2004)

The Validity of Using the Microscopic Parabolic Heat Conduction Model in Place of the Macroscopic Parabolic Model under the Effect of a Moving Heating Source

A. F. Khadrawi[1] **and M. A. Al-Nimr**[2, 3]

Received July 22, 2003

The validity of the use of the microscopic parabolic heat conduction model under the effect of a moving heating source is investigated. Two configurations are considered which are the finite and the semi-infinite domains. For each configuration, two types of thermal boundary conditions are considered which are the isothermal and the insulated types. Four dimensionless parameters are found to control the thermal behavior of the considered problem which are the dimensionless heating source speed U, heat capacity ratio C_R, dimensionless amplitude of the heating source S_0, and dimensionless plate thickness ξ_0 for the finite domain configuration. It is found that the use of the microscopic parabolic heat conduction model instead of the parabolic macroscopic model is essential when the dimensionless speed of the source $U > 0.1$ The heat capacity ratio C_R is found to have insignificant effect on the domain thermal behavior. However, the deviation between the microscopic and macroscopic models increases as ξ_0 decreases. The deviation between the two models is significant within the very early stages of time.

KEY WORDS: heat conduction; microscopic parabolic model; moving source; two-step model; validation criterion.

1. INTRODUCTION

Energy transport during high-rate heating of thin metal films is a rapidly emerging area in heat transfer [1–11]. When a thin film is exposed to a

[1] Mechanical Engineering Department, Al-Balqa' Applied University, Al-Salt, Jordan.
[2] Mechanical Engineering Department, Jordan University of Science and Technology, P.O. Box 3030, Irbid 22210, Jordan.
[3] To whom correspondence should be addressed. E-mail: malnimr@just.edu.jo

0195-928X/04/0500-0931/0

very rapid heating process, such as that induced by a short-pulse laser, the response time of the film is typically of the order of 1 ps, which is comparable to the phonon–electron thermal relaxation time. Under these situations, thermal equilibrium between a solid lattice and electron gas cannot be assumed and heat transfer in the electron gas and the metal lattice needs to be considered separately. Models describing the nonequilibrium thermal behavior in such cases are called the microscopic two-step models. Two microscopic heat conduction models are available in the literature. The first one is the parabolic two-step model [1–5, 8–11], and the second one is the hyperbolic two-step model [1, 3, 7].

Ultrafast heating of metals consists of two major steps of energy transfer that occur simultaneously. In the first step, electrons absorb most of the incident radiation energy and the excited electron gas transmits its energy to the lattice through an inelastic electron–phonon scattering process [1–3]. In the second step, the incident radiation absorbed by the metal film diffuses spatially within the film mainly by the electron gas. For typical metals, depending on the degree of electron–phonon coupling, it takes about 0.1–1 ps for electrons and a lattice to reach thermal equilibrium. When the ultrafast heating pulse duration is comparable with or less than this thermal equilibration time, the electrons and lattice are not in thermal equilibrium.

In the literature, numerous studies have been conducted using the microscopic parabolic heat conduction model [1–5, 8–11]. These studies show that use of this model is a necessity in applications involving very thin film, very short duration heating sources, and very high frequency fluctuating heating sources. In the present work, we intend to investigate the thermal behavior of metal films under the effect of a moving plane surface heating source.

The heating source will heat the electron gas, which in turn exchanges part of its energy with the solid lattice. In applications involving heating sources with very high velocity, there is not enough time available for the electron gas and solid lattice to attain the same temperature. The goal of the present work is to investigate the conditions under which the use of the microscopic parabolic heat conduction model in place of the macroscopic heat conduction model is a necessity.

Two configurations are considered which are the finite and semi-infinite domains. Also, two types of thermal boundary conditions are considered with each configuration, which are the insulated and isothermal boundary conditions.

2. ANALYSIS

Referring to Fig. 1, we consider finite (Fig. 1a) and semi-infinite (Fig. 1b) domains, which have an initial temperature equal to the ambient value. Suddenly, a moving plane surface heat source starts moving within each domain. The source starts its motion from the plate centerline in the case of the finite domain and from the surface in the case of the semi-infinite domain. Using the dimensionless parameters given in the nomenclature, the governing equation of the parabolic heat conduction model is given as

$$\frac{\partial \theta_e}{\partial \eta} = \frac{\partial^2 \theta_e}{\partial \xi^2} - (\theta_e - \theta_l) + \frac{S_0}{U}\delta\left(\eta - \frac{\xi}{U}\right), \tag{1}$$

$$\frac{\partial \theta_l}{\partial \eta} = C_R(\theta_e - \theta_l). \tag{2}$$

When the electron and lattice temperatures are very close to each other, the microscopic parabolic heat conduction model may be replaced with the macroscopic parabolic heat conduction model, which assumes that $\theta_e = \theta_l = \theta$, as

$$\frac{\partial \theta}{\partial \eta} = \frac{\partial^2 \theta}{\partial \xi^2} + \frac{S_0}{U}\delta\left(\eta - \frac{\xi}{U}\right). \tag{3}$$

Equations (1) and (2) have the following initial conditions:

$$\theta_e(0, \xi) = \theta_l(0, \xi) = 0.$$

The boundary conditions depend on the type of configuration and they are given as

Configuration (1): Infinite domain

(A) Insulated boundary condition:

$$\frac{\partial \theta_e}{\partial \xi}(\eta, 0) = \frac{\partial \theta_l}{\partial \xi}(\eta, 0) = 0, \quad \theta_e(\eta, \infty) = \theta_l(\eta, \infty) = 0. \tag{4a}$$

(B) Isothermal boundary condition:

$$\theta_e(\eta, 0) = \theta_l(\eta, 0) = 0, \quad \theta_e(\eta, \infty) = \theta_l(\eta, \infty) = 0. \tag{4b}$$

Configuration (2): Finite domain

(A) Insulated boundary condition:

$$\frac{\partial \theta_e}{\partial \xi}(\eta, 0) = \frac{\partial \theta_l}{\partial \xi}(\eta, 0) = 0, \quad \frac{\partial \theta_e}{\partial \xi}(\eta, \xi_0) = \frac{\partial \theta_l}{\partial \xi}(\eta, \xi_0) = 0. \tag{4c}$$

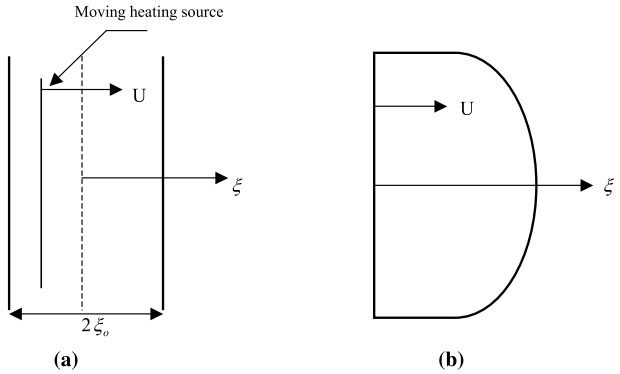

Fig. 1. Schematic diagram of the problem under consideration.

(B) Isothermal boundary condition:

$$\frac{\partial \theta_e}{\partial \xi}(\eta, 0) = \frac{\partial \theta_l}{\partial \xi}(\eta, 0) = 0, \quad \theta_e(\eta, \xi_0) = \theta_l(\eta, \xi_0) = 0. \tag{4d}$$

Equations (1) and (2) are solved using the Laplace transformation technique. Now with the notation that $L\{\theta_e(\eta, \xi)\} = W_e(S, \xi)$ and $L\{\theta_l(\eta, \xi)\} = W_l(S, \xi)$, the Laplace transformation of Eqs. (1) and (2) yields

$$SW_e = \frac{d^2 W_e}{d\xi^2} - W_e + W_l + \frac{S_0}{U} e^{-\frac{S\xi}{U}}, \tag{5}$$

$$SW_l = C_R W_e + C_R W_l. \tag{6}$$

Also, the Laplace transformation of the boundary conditions is given as
Configuration (1): Infinite domain

(A) Insulated boundary condition:

$$\frac{\partial W_e}{\partial \xi}(S, 0) = \frac{\partial W_l}{\partial \xi}(S, 0) = 0, \quad W_e(S, \infty) = W_l(S, \infty) = 0. \tag{7a}$$

(B) Isothermal boundary condition:

$$W_e(S, 0) = W_l(S, 0) = 0, \quad W_e(S, \infty) = W_l(S, \infty) = 0. \tag{7b}$$

Configuration (2): Finite domain

(A) Insulated boundary condition:

$$\frac{\partial W_e}{\partial \xi}(S, 0) = \frac{\partial W_l}{\partial \xi}(S, 0) = 0, \quad \frac{\partial W_e}{\partial \xi}(S, \xi_0) = \frac{\partial W_l}{\partial \xi}(S, \xi_0) = 0. \tag{7c}$$

(B) Isothermal boundary condition:

$$\frac{\partial W_e}{\partial \xi}(S,0)=\frac{\partial W_1}{\partial \xi}(S,0)=0, \quad W_e(S,\xi_0)=W_1(S,\xi_0)=0. \tag{7d}$$

Equations (5) and (6) assume the following solutions for W_e and W_1:
Configuration (1): Infinite domain

$$W_e(S,\xi) = De^{-\frac{S\xi}{U}} + Ee^{-\beta\xi}, \tag{8}$$

$$W_1(S,\xi) = \frac{C_R W_e}{S+C_R}. \tag{9}$$

Configuration (2): Finite domain

$$W_e(S,\xi) = E\cosh(\beta\xi) + F\sinh(\beta\xi) + De^{-\frac{S\xi}{U}}, \tag{10}$$

$$W_1(S,\xi) = \frac{C_R W_e}{S+C_R}, \tag{11}$$

where $\beta=\sqrt{1+S-\frac{C_R}{S+C_R}}$.

The constants E, F, and D assume values depend on the type of configuration and thermal boundary condition and are given as
Infinite domain with insulated boundaries:

$$D=\frac{S_0}{\left(\beta^2-\frac{S^2}{U^2}\right)U} \quad \text{and} \quad E=\frac{-DS}{\beta U}.$$

Infinite domain with isothermal boundaries:

$$D=\frac{S_0}{\left(\beta^2-\frac{S^2}{U^2}\right)U} \quad \text{and} \quad E=-D.$$

Finite domain with insulated boundaries:

$$E=\frac{\frac{DS}{U}e^{-\frac{S\xi_0}{U}}-F\beta\cosh(\beta\xi_0)}{\beta\sinh(\beta\xi_0)}, \quad F=\frac{DS}{\beta U} \quad \text{and} \quad D=\frac{S_0}{\left(\beta^2-\frac{S^2}{U^2}\right)U}.$$

Finite domain with isothermal boundaries:

$$E=-D, \quad F=\frac{-De^{-\frac{S\xi_0}{U}}-E\cosh(\beta\xi_0)}{\sinh(\beta\xi_0)} \quad \text{and} \quad D=\frac{S_0}{\left(\beta^2-\frac{S^2}{U^2}\right)U}.$$

Equations (8)–(11) are inverted using a computer program based on the Riemann-sum approximation [1] as

$$\theta(\eta,\xi)\cong\frac{e^{\gamma\eta}}{\eta}\left[\frac{1}{2}W(\gamma,\xi)+\mathrm{Re}\sum_{n=1}^{N}W\left(\gamma+\frac{in\pi}{\eta},\xi\right)(-1)^n\right],$$

where Re refers to the "real part of," i is the imaginary number $\sqrt{-1}$, and γ is the real part of the Bromwich contour that is used in inverting Laplace transforms. For faster convergence, the quantity $\gamma\eta=4.7$ gives the most satisfactory results. The quantity $\gamma\eta=4.7$ is found to be appropriate in our case since other tested values of $\gamma\eta$ seem to need longer computational time.

2.1. Thermal Shock Wave Phenomenon

One of the interesting phenomena in the parabolic two-step heat conduction model is the possible formation of the thermal shock wave. When the heat source moves at a speed equal to or faster than that of the heat propagation in the solid, a large amount of thermal energy accumulates in the neighborhood of the moving heat source. Such accumulated energy cannot be efficiently transferred to the surrounding media before the heat source moves away. To examine this phenomenon in the parabolic two-step model, the governing equation for the lattice temperature in dimensional form is expressed as:

$$\frac{\partial^2 T_l}{\partial x^2}+\frac{\alpha_e}{C_E^2}\frac{\partial^3 T_l}{\partial t\,\partial x^2}=\frac{1}{\alpha_e}\frac{\partial T_l}{\partial t}+\frac{1}{C_E^2}\frac{\partial^2 T_l}{\partial t^2}. \tag{12}$$

The thermal diffusivity of the electron gas α_e, is defined by $\frac{k}{C_e}$. The equivalent thermal diffusivity α_E and thermal wave speed C_E in such a phonon–electron system are defined as

$$\alpha_E=\frac{k}{C_e+C_l},\quad C_E=\sqrt{\frac{kG}{C_eC_l}}.$$

Table I shows the equivalent thermal wave speed C_E and the corresponding dimensionless equivalent thermal wave speed U_E, which is equal to $\sqrt{\frac{C_e}{C_l}}$, for many metals.

Table I. Equivalent Thermal Wave Speed and Corresponding Dimensionless Equivalent Thermal Wave Speed

Metal	Equivalent thermal wave speed $C_E(\mathrm{m}\cdot\mathrm{s}^{-1})$	Dimensionless equivalent thermal wave speed U_E
Cu	1.6109×10^4	0.0786
Ag	1.4949×10^4	0.0917
Au	1.2961×10^4	0.0917
Pb	1.1738×10^4	0.1183

3. RESULTS AND DISCUSSION

The interest is focused on the operating conditions to validate the usage of the macroscopic parabolic heat conduction model instead of the microscopic parabolic one. This is done by tracing the effect of different dimensionless parameters on the difference between the electron and lattice temperatures $(\theta_e - \theta_l)$. These dimensionless parameters are found to be U, C_R and ξ_0. However, it is found better to normalize the temperature difference $(\theta_e - \theta_l)$ by multiplying it by U/S_0, and as a result, the normalized temperature difference is given as $(\theta_e - \theta_l)\, U/S_0$. The reason for creating such a normalized temperature difference is to give a sort of relative deviation between θ_e and θ_l instead of the absolute difference. To explain this, it is known that the total amount of energy released by the moving source decreases as U increases. As a result, both the electron and lattice temperatures decrease and the absolute difference between them $|\theta_e - \theta_l|$ also decreases. This small difference between θ_e and θ_l at high U may give a wrong impression that the macroscopic heat conduction model is valid, which is not true. In this case it is better to search for a sort of percentage relative difference, which is found in the normalized quantity $|\theta_e - \theta_l|\, U/S_0$. Other possibilities include to divide the difference $|\theta_e - \theta_l|$ by θ_e or θ_l, but in such a case, there is a problem for locations that do not feel the effect of the moving heating source and that have zero temperatures for both θ_e and θ_l.

Figures 2–8 show the validity of the use of the macroscopic parabolic heat conduction model in a semi-infinite domain with insulated and isothermal surfaces, while Figs. 9–12 consider the case of a finite domain with insulated and isothermal surfaces.

Figure 2 shows the spatial distribution of the normalized temperature difference between θ_e and θ_l at a different heating source velocity U. As clear from this figure, the normalized difference increases as U increases. Also, it is clear from Figs. 3 to 4 that the normalized difference

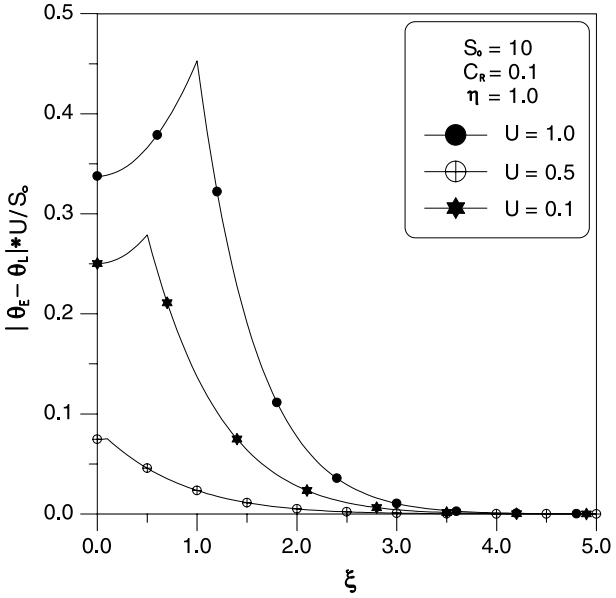

Fig. 2. Spatial distribution of the normalized temperature difference between θ_e and θ_l at different U (semi-infinite, insulated).

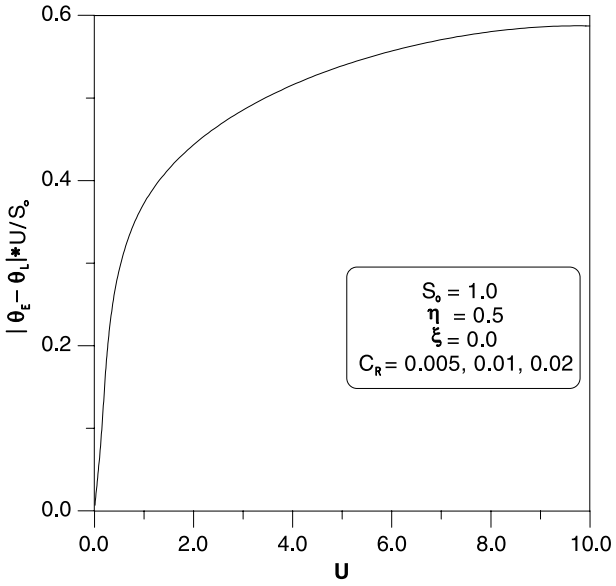

Fig. 3. Effect of U on the normalized temperature difference between θ_e and θ_l at different C_R (semi-infinite, insulated).

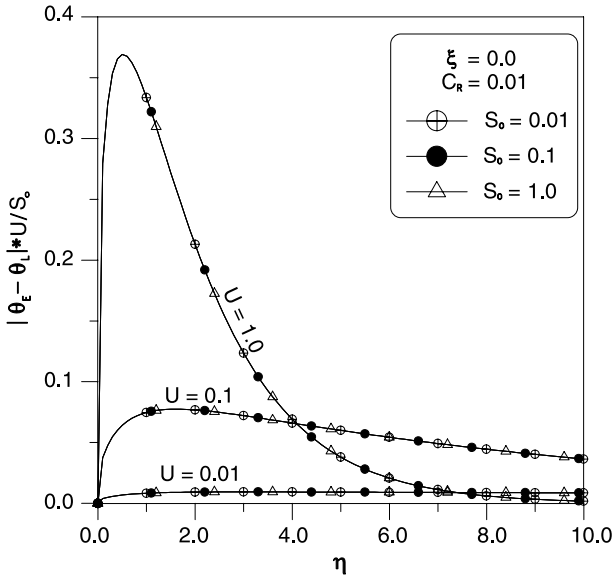

Fig. 4. Effect of S_0 on the transient behavior of the normalized temperature difference between θ_e and θ_l (semi-infinite, insulated).

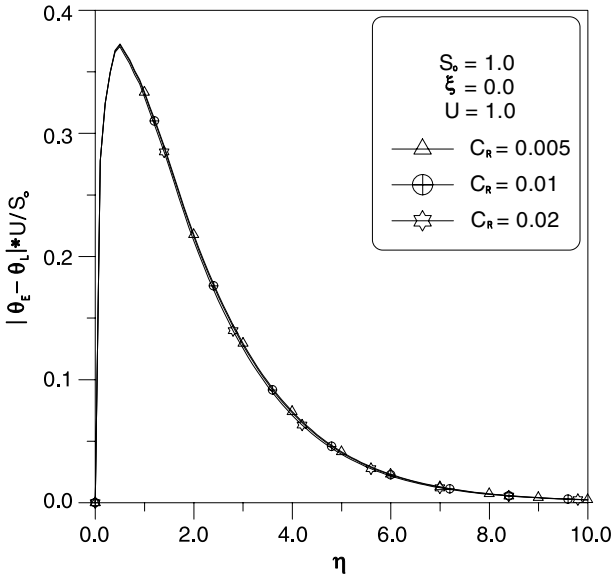

Fig. 5. Effect of C_R on the transient behavior of the normalized temperature difference between θ_e and θ_l (semi-infinite, insulated).

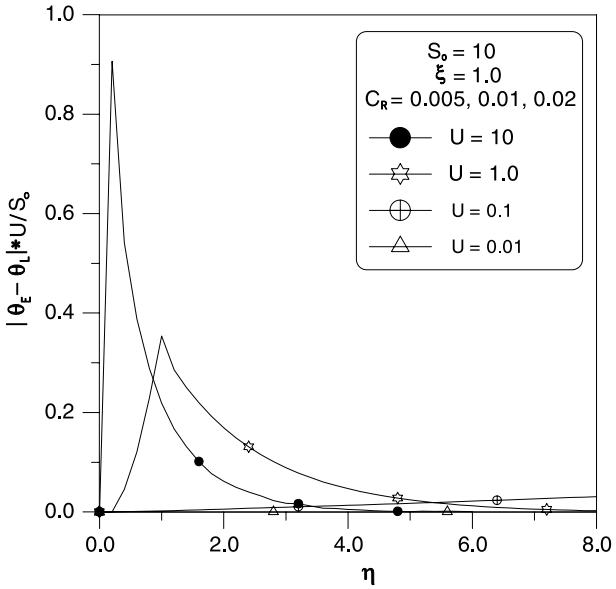

Fig. 6. Effect of U on the transient behavior of the normalized temperature difference between θ_e and θ_l (semi-infinite, isothermal).

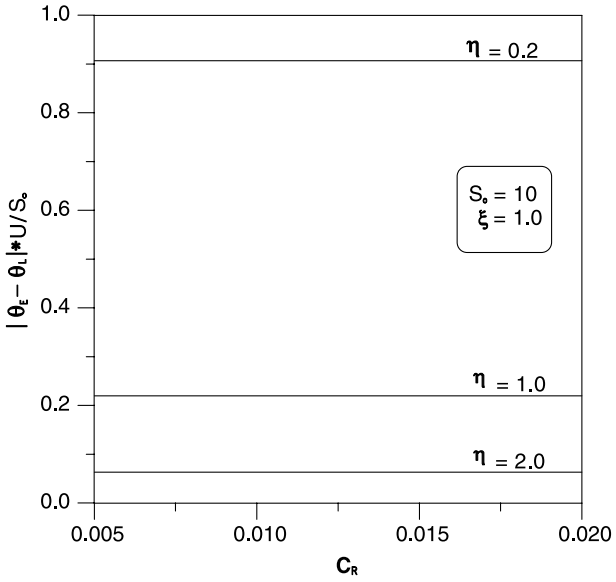

Fig. 7. Effect of C_R on the normalized temperature difference between θ_e and θ_l at different η (semi-infinite, isothermal).

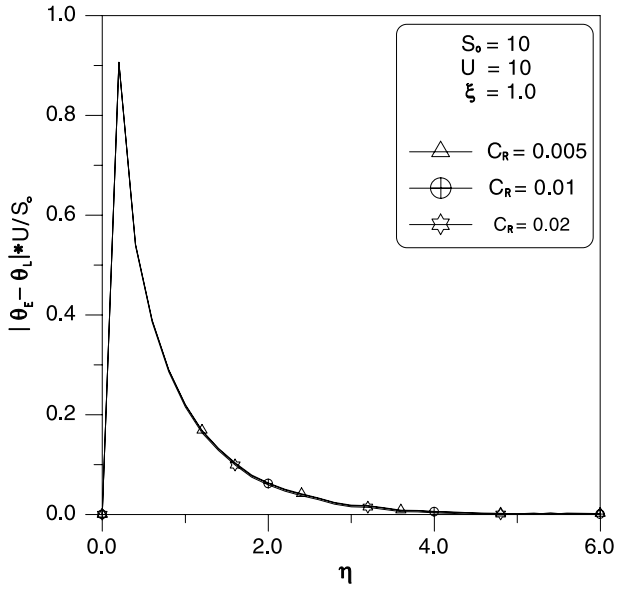

Fig. 8. Effect of C_R on the transient behavior of the normalized temperature difference between θ_e and θ_l (semi-infinite, isothermal).

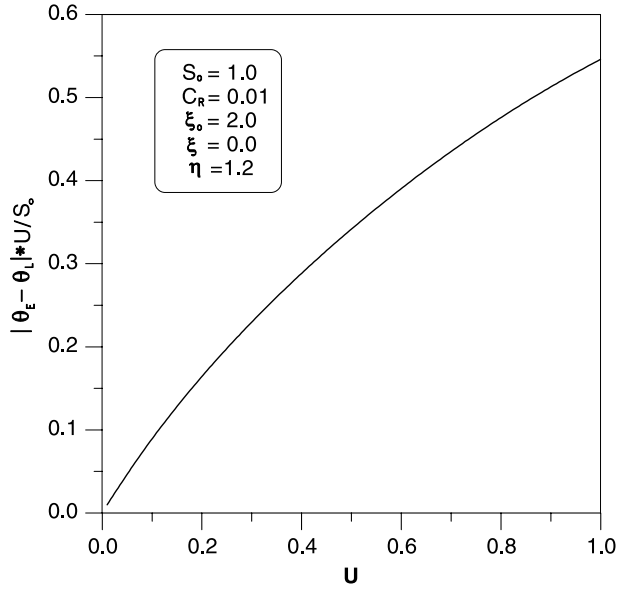

Fig. 9. Effect of U on the normalized temperature difference (finite, insulated).

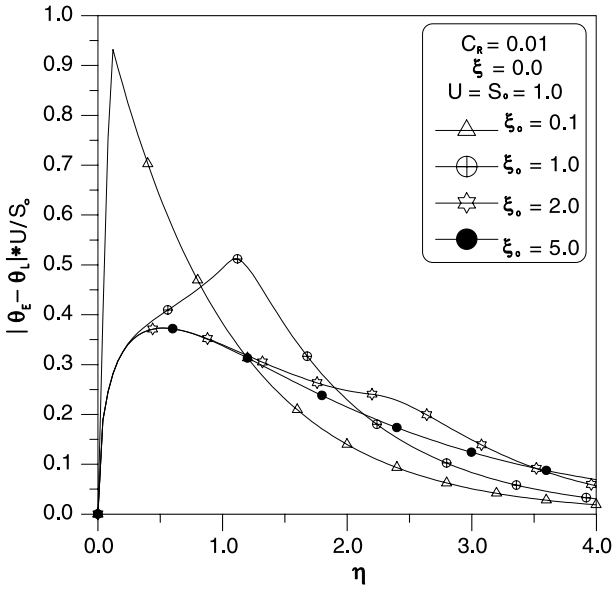

Fig. 10. Effect of ξ_0 on the transient behavior of the normalized temperature difference between θ_e and θ_l (finite, insulated).

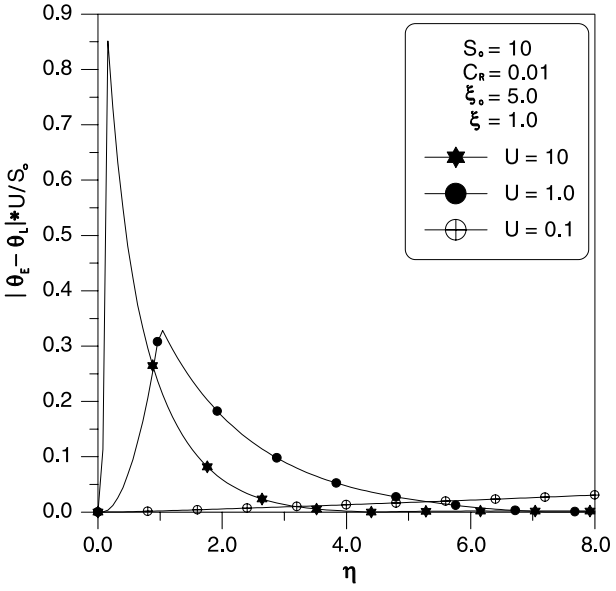

Fig. 11. Effect of U on the transient behavior of the normalized temperature difference between θ_e and θ_l (finite, isothermal).

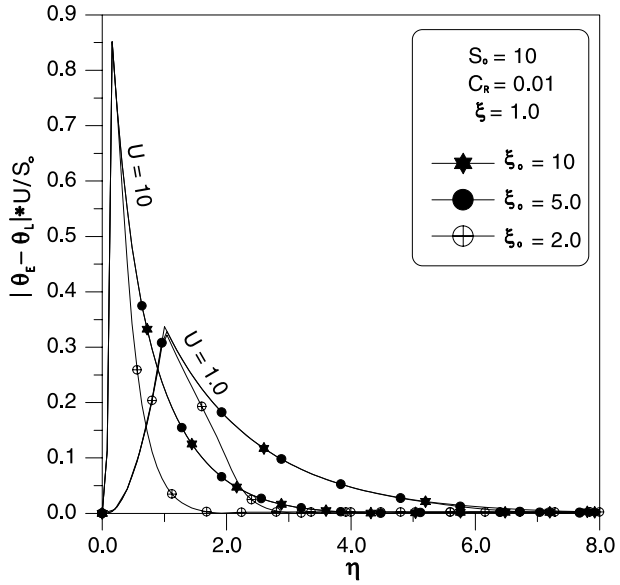

Fig. 12. Effect of ξ_0 on the transient behavior of the normalized temperature difference between θ_e and θ_l (finite, isothermal).

increases as U increases and it is essential to use the microscopic model for moving sources have $U > 0.1$. Most typical thin metals have G of order $10^{16}\,\mathrm{W \cdot m^{-3} \cdot K^{-1}}$, C_e of order $10^4\,\mathrm{J \cdot m^{-3} \cdot K^{-1}}$, and k_e of order $100\,\mathrm{W \cdot m^{-1} \cdot K^{-1}}$. This implies that the use of the microscopic heat conduction model is essential when u is larger than $10^4\,\mathrm{m \cdot s^{-1}}$. Under the effect of a high speed moving source, the time available for the electron and lattice to exchange heat has the same order of magnitude as the time required by the electron gas to receive heat from the ultrafast moving heating source. The peak in the normalized temperature difference becomes sharp and high as U increases, and this peak moves toward larger times as U decreases, and in the limit of very small U, such a peak diminishes as shown in Fig. 4. This implies that the use of the microscopic parabolic heat conduction model is essential in the early stages of time. Also, the dimensionless amplitude of the heating source S_0 has an insignificant effect on the normalized temperature difference.

Figure 5 shows the effect of C_R on the transient behavior of the normalized temperature difference. For most known metals, C_R varies within a very narrow range (0.005 – 0.02) and the effect of C_R within this narrow range on the normalized temperature difference is insignificant.

Figure 6 shows the effect of U on the normalized temperature difference for the isothermal case. Conclusions similar to that of Fig. 4 may

be obtained with very slight difference in the thermal behavior. Also, the effect of C_R on the normalized temperature difference in a semi-infinite domain with an isothermal surface is shown in Figs. 7 and 8. Again, the main conclusions drawn for the insulated case remain the same.

Figures 9 and 10 show the effect of different parameters on the normalized temperature difference in a finite domain of thickness ξ_0 having insulated surfaces. Here, ξ_0 is a new effective parameter, which has not been seen in a semi-infinite case.

Figure 9 shows the effect of U on the normalized temperature difference between θ_e and θ_l. Again, the use of the microscopic parabolic heat conduction model is essential when $U > 0.1$ and this conclusion is similar to a semi-infinite case. Other observations are similar to that found in Figs. 3 and 4.

Figure 10 shows the effect of ξ_0 on the dynamic behavior of the normalized temperature difference. It is clear that the peaks in the normalized temperature difference increases as ξ_0 decreases. This implies that the use of the microscopic parabolic heat conduction model is essential in thin metal films independent of the value of other different parameters. Again, the peaks in the normalized temperature difference appear within the early stages of times and this implies that the use of the microscopic heat conduction model is essential to predict the metal thermal behavior within the early stages of time.

Figure 11 shows the effect of U on the normalized temperature difference between θ_e and θ_l for the isothermal case. Again, the use of the microscopic parabolic heat conduction model is essential when $U > 0.1$ and this conclusion is similar to that for the semi-infinite case. Other observations are similar to that found in Figs. 4 and 6.

Figure 12 shows the effect of ξ_0 on the dynamic behavior of the normalized temperature difference at different U's. The peak in the normalized temperature difference becomes sharp and high as U increases and this peak moves toward larger times as U decreases. This implies that the use of the microscopic parabolic heat conduction model is essential in the early stages of time. Also, it is clear that the effect of ξ_0 on the normalized temperature difference is insignificant.

Figures 13 and 14 show the transient response of the dimensionless lattice temperatures at three velocities and for two metals. Each figure consists of three curves where each curve corresponds to a specific speed of the moving heating source. These speeds are selected such that one is slightly slower, the second is exactly equal to, and the third is slightly faster than the equivalent wave speed in phonon–electron interactions. It is clear that the thermal shock wave phenomenon does not appear in these figures due to the fact that the total amount of energy released by

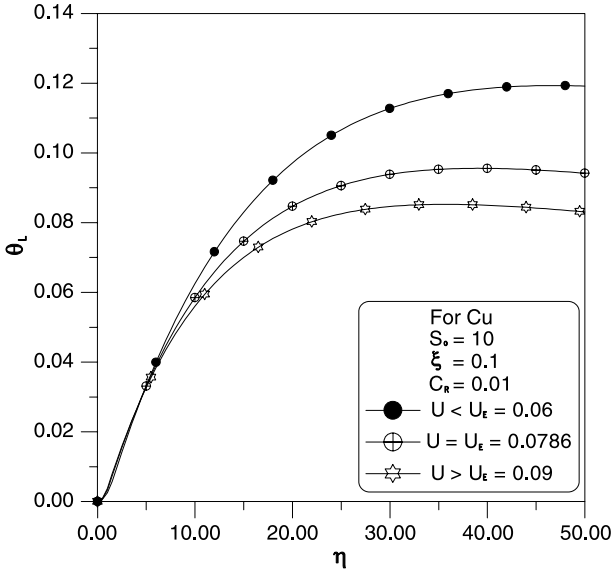

Fig. 13. Transient response of the dimensionless lattice temperature at different U for Cu.

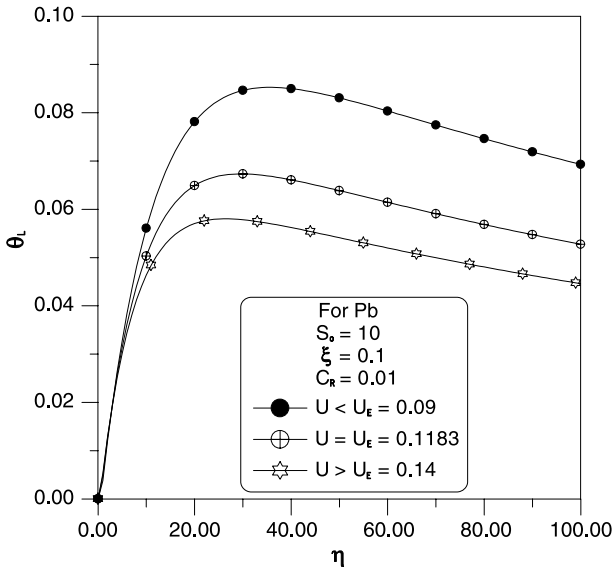

Fig. 14. Transient response of the dimensionless lattice temperature at different U for Pb.

the moving source decreases as U increases. This implies that the slight increase in the lattice temperature due to the accumulation of energy at the wave front is overshadowed by the decrease in this energy due to the increase in the moving source speed. Also, in reality, the thermal wave has a speed different than the equivalent thermal wave speed. It may be better to consider a point heating source rather than a plane heat source to trace the thermal shock phenomenon. With a point heat source it is possible to observe the variation in the lattice temperature within the circumference of the continuum circle centered at the heat source.

4. CONCLUSION

The validity of the use of the macroscopic parabolic heat conduction model instead of the microscopic hyperbolic model is investigated under the effect of a moving heating source. Two configurations are considered which are the finite and semi-infinite domains, and two thermal boundary conditions are considered for each configuration, which are the insulated and isothermal boundary conditions. Four dimensionless parameters are found to affect the domain thermal behavior, which are U, C_R, S_0, and ξ_0. It is found that the use of the microscopic parabolic heat conduction model is essential in domains containing heating sources that move with $U > 0.1$ The effect of the heat capacity ratio C_R and the dimensionless amplitude of the heating source S_0 on the domain thermal behavior is found to be insignificant. On the other hand, the use of the microscopic parabolic heat conduction model is found to be essential during the early stages of time and in very thin domains except in a finite domain with an isothermal boundary.

NOMENCLATURE

C	heat capacity, $\mathrm{J \cdot m^{-3} \cdot K^{-1}}$
C_E	equivalent thermal wave speed, $\sqrt{kG/C_e C_l}$
C_R	heat capacity ratio, C_e/C_l
G	electron-phonon coupling factor, $\mathrm{J \cdot m^{-3} \cdot K^{-1}}$
K	thermal conductivity, $\mathrm{W \cdot m^{-1} \cdot K^{-1}}$
q	conduction heat flux, $\mathrm{W \cdot m^{-2}}$
Q	dimensionless conduction heat flux, $q\sqrt{k_e/G/kT_\infty}$
S	Laplacian domain
s_e	volumetric heating source, $\mathrm{W \cdot m^{-3}}$
s_0	amplitude of the heating source, $\mathrm{W \cdot m^{-2}}$
S_0	dimensionless amplitude of the heating source, $s_0/GT_\infty\sqrt{k_e/G}$
t	time, s

T temperature, K
T_∞ ambient and initial temperature, K
u velocity of heating source, $\mathrm{m}\cdot\mathrm{s}^{-1}$
U dimensionless velocity of heating source velocity, $uC_\mathrm{e}/\sqrt{Gk_\mathrm{e}}$
U_E dimensionless equivalent thermal wave speed, $\sqrt{C_\mathrm{e}/C_\mathrm{l}}$
x transverse coordinate, m
$2x_0$ plate thickness

Greek symbols

α thermal diffusivity, k/C
α_E equivalent thermal diffusivity, $k/(C_\mathrm{e}+C_\mathrm{l})$
δ Dirac's delta function
η dimensionless time, tG/C_e
θ dimensionless temperature, $(T-T_\infty)/T_\infty$
ξ dimensionless transverse coordinate, $x/\sqrt{k_\mathrm{e}/G}$
ξ_0 dimensionless thickness of the plate, $x_0/\sqrt{k_\mathrm{e}/G}$

Subscript

e electron gas
F Fermi surface
l solid lattice
∞ ambient

REFERENCES

1. D. Y. Tzou, in *Macro-to-Microscale Heat Transfers-The Lagging Behavior* (Taylor and Francis, New York, 1997), pp. 1–64.
2. T. Q. Qiu and C. L. Tien, *Int. J. Heat Mass Transfer* **35**:719 (1992).
3. T. Q. Qiu and C. L. Tien, *J. Heat Transfer* **115**:835 (1993).
4. S. L. Anisimov, B. L. Kapeliovich, and T. L. Perelman, *Sov. Phys. JETP* **39**:375 (1974).
5. J. G. Fujimoto. J. M. Liu, and E. P. Ippen, *Phys. Rev. Lett.* **53**:1737 (1984).
6. D. Y. Tzou, *J. Heat Transfer* **117**:8 (1995).
7. M. A. Al-Nimr and V. S. Arpaci, *Int. J. Heat Mass Transfer* **43**:2021 (2000).
8. M. A. Al-Nimr and V. S. Arpaci, *J. Appl. Phys.* **85**:2517 (1999).
9. M. A. Al-Nimr and S. Masoud, *ASME J. Heat Transfer* **119**:188 (1997).
10. M. A. Al-Nimr, *Int. J. Thermophys.* **18**:1257 (1997).
11. S. Kiwan and M. A. Al-Nimr, *Jpn. J. Appl. Phys.* **39**:4245 (2000).